



# Predicting iron deficiency and oxidative stress in *Glycine max* through Fourier transform infrared spectroscopy in a time-course experiment

Carla S. Santos · Clara Sousa · Maryam Bagheri ·  
Simão Pinho · Marta W. Vasconcelos

Received: 15 December 2022 / Accepted: 23 June 2023  
© The Author(s) 2023

## Abstract

**Aims** The excessive use of fertilizers is a problem in current agricultural systems, and sustainable farming practices, including precision agriculture, demand the use of new technologies to manage plant stress at an early stage. To sustainably manage iron (Fe) fertilization in agricultural fields, it is urgent to develop early detection methods for Fe deficiency, and linked oxidative stress, in plant leaves. Herein, the potential of using Fourier Transform Infrared (FTIR) spectroscopy for Fe deficiency and oxidative stress detection in soybean plants was evaluated.

**Methods** After a period of two weeks of hydroponic growth under optimum conditions, soybean plants were grown under Fe-sufficient (Fe+) and Fe-deficient (Fe-) hydroponic conditions for four weeks. Sampling occurred every week, infrared (IR) spectra were acquired and biological parameters (total chlorophyll, anthocyanins and carotenoids concentration,

and ABTS and DPPH free radical scavenging ability), mineral concentrations, and the Fe-related genes' expression - *FRO2*- and *IRT1*-like - were evaluated.

**Results** Two weeks after imposing Fe deficiency, plants displayed decreased antioxidant activity, and increased expression levels of *FRO2*- and *IRT1*-like genes. Regarding the PLS models developed to estimate the biological parameters and mineral concentrations, satisfactory calibration models were globally obtained with R<sup>2</sup>C from 0.93 to 0.99. FTIR spectroscopy was also able to discriminate between Fe+ and Fe- plants from an early stage of stress induction with 96.3% of correct assignments.

**Conclusion** High reproducibility was observed among the different spectra of each sample and FTIR spectroscopy may be an early, non-invasive, cheap, and environmentally friendly technique for IDC management.

**Keywords** Chemometrics · Ferric reductase oxidase · iron regulated transporter · Legumes · Oxidative stress · Photosynthetic pigments

Responsible Editor: Stefano Cesco.

**Supplementary information** The online version contains supplementary material available at <https://doi.org/10.1007/s11104-023-06143-y>.

C. S. Santos · C. Sousa · M. Bagheri · S. Pinho ·  
M. W. Vasconcelos (✉)  
CBQF – Centro de Biotecnologia e Química Fina –  
Laboratório Associado, Escola Superior de Biotecnologia,  
Universidade Católica Portuguesa, Rua Diogo Botelho  
1327, 4169-005 Porto, Portugal  
e-mail: mvasconcelos@ucp.pt

## Introduction

Soybean [*Glycine max* (L.) Merr.] is an oil crop with a high economic impact worldwide. It had an estimated harvested area of 127 million hectares and a total world production of 353 million metric tonnes in 2020 (FAO 2022). Soybean has multiple food and

feed applications and it is a major source of protein and minerals, particularly in the rising dietary trends as a meat and dairy alternative (Messina et al. 2022).

Iron (Fe) is an essential micronutrient for plant growth and maturation, photosynthesis, respiration, nitrogen fixation, hormone production, and DNA synthesis (Celletti et al. 2020; Guerinot and Yi 1994). It is necessary for chlorophyll and other photosynthetic pigments biosynthesis (Prasad 2003) and is a constituent of the electron transport chain in mitochondria and chloroplasts (Mittler et al. 2004). However, in areas where calcareous soils prevail, Fe bioavailability is hindered due to reduced solubility leading to the development of Iron Deficiency Chlorosis (IDC) (Chaney 2022). Soybean plants are particularly affected by IDC (Peiffer et al. 2012). This condition is characterized by the yellowing or necrosis of the leaves, stunted growth, yield loss, and, ultimately, plants' death (Prasad 2003). It is a current leading factor of great economic losses both to growers and breeders (Xu et al. 2021).

In dicotyledonous plants, Fe uptake involves the reduction of the insoluble Fe(III) in the soil to Fe(II) through the activity of a membrane-bound ferric reductase, such as the Ferric Reductase Oxidase 2 (FRO2). After the reduction step, Fe(II) is taken up to the root epidermal cells via Fe transporters, such as the Iron-Regulated Transporter 1 (IRT1) (Jeong and Connolly 2009). The process of Fe absorption is highly affected by multiple factors (e.g. genetic, physiological), which determine the plants' efficiency to induce biochemical (García-Mina et al. 2013) and molecular (Riaz and Guerinot 2021; Santos et al. 2019a) reactions that make Fe more available for uptake. Specifically, the biochemical responses to Fe stress include reduced photosynthetic rate, due to the fact that chloroplasts are major Fe sink organelles and contain up to 90% of foliar Fe (Akmakjian et al. 2021); changes in the activity of enzymes related to plant growth pathways and acid organic metabolism (Ceballos-Laita et al. 2015; Jelali et al. 2010, Zhitkovich 2021), impairing plant's development and the ability to respond to stress; changes in cell wall composition, related to the fact that Fe is involved in lignin synthesis, ultimately affecting mineral balances and distribution in the plant (Rodríguez-Celma et al. 2016); and alterations in the synthesis of hormones, which may act as signalling molecules to trigger Fe deficiency responses (García et al. 2022). Micro and

macronutrients are also deeply affected by Fe deficiency. This condition impacts nutrient distribution within the plant, particularly in younger leaves, thus impairing plant growth and development (García-Molina et al. 2020; Santos et al. 2015). It also leads to the decrease in the amount of nitrogen and sulphur-containing amino acids which are essential for protein synthesis (Borlotti et al. 2012; Cheng et al. 2019).

Additionally, studies show that Fe-deficient plants produce higher levels of reactive oxygen species (ROS) given that Fe is a co-factor of many antioxidant enzymes (Santos et al. 2019b; Singh and Bhatla 2022). ROS may act as signalling molecules for Fe deficiency (Santos et al. 2019b; Sun et al. 2016; García-Caparrós et al. 2021), and the early detection of oxidative stress may be an important tool to diagnose and improve plant tolerance to Fe deficiency.

The most common method to cope with IDC at the production level is the application of Fe–chelates, such as ethylenediaminetetraacetic acid (EDTA) and ethylenediamine di(o-hydroxyphenyl acetic) acid (EDDHA) (García-Marco et al. 2006). In light of current societal changes and the climate change effects, global food security is at risk (Feliciano et al. 2022; Hassen and Bilali 2022). It is, therefore, critical to develop and establish methods that contribute to a sustainable and precise management of mineral deficiencies in the field (precision agriculture), which will have both an impact on the economic balance of crop production, and on the cost of fertilizers applied to the environment (Breure et al. 2022). In this context, spectroscopic techniques are being increasingly studied and tested in plant health diagnosis, as they avoid time-consuming processing and allow high-throughput analysis (Lima et al. 2014; Ncube et al. 2022).

Fourier transform infrared (FTIR) spectroscopy allows the acquisition of information with no need for organic reagents and time-consuming sample preparation techniques (Lahlali et al. 2014). Additionally, when coupled with the Attenuated Total Reflection (ATR) sampling mode, it presents a clear advantage of not needing any sample preparation step and being non-destructive (Butler et al. 2015). Using FTIR spectroscopy, proteins, lipids, carbohydrates, and nucleic acids can be screened, allowing for the detection of structural and biochemical changes that may occur in plants after a stress condition (McCann et al. 1992; Osman et al. 2022). This spectroscopic

technique has been used for several purposes in the context of plant stress characterization; namely, for detecting biomolecular changes influenced by water deficit stress in *Physalis peruviana* (Leite et al. 2022) and soybean (Hlahla et al. 2022); searching for new biomarkers to diagnose heat-stress leaves in pea (Liu et al. 2019) and in wheat (Osman et al. 2022); and characterising physiological, biochemical and molecular responses of different plants to salt stress (Mehmood et al. 2020; Nikalje et al. 2019) and heavy metal toxicity (Yu et al. 2020).

Despite all of this evidence, the application of FTIR spectroscopy to study Fe deficiency response in soybean plants is yet to be reported. Also, the degree of predictability between FTIR spectra and specific biochemical traits related to Fe deficiency responses is not known. Hence, in this study, it was hypothesized that FTIR spectroscopy is a suitable technique for IDC early detection, with low environmental and economic costs, based on the alteration of the spectral reflectance properties of soybean plant leaves, caused by Fe stress. To test this hypothesis, the leaves of soybean plants grown under Fe sufficient and Fe deficient hydroponic conditions, were monitored for total chlorophyll, anthocyanins and carotenoids, anti-oxidant response, FRO2 and IRT1 expression, and mineral accumulation. Data modelling was performed to integrate the physiological and biochemical data with the infrared (IR) spectra, aiming to understand the ability of this technique to differentiate between plants grown under different Fe regimens and to predict chlorophyll concentration, ABTS and DPPH free radical scavenging ability and mineral concentrations.

## Materials and methods

### Plant material, growth conditions, and treatments

Seeds of the *G. max* cultivar “Williams 82” were germinated for seven days in the dark at 25 °C on moist paper. Germinated seedlings were transferred to 10 L vessels adapted for hydroponic growth (10 seedlings per vessel). The vessels were placed in a climate chamber (Aralab Fitoclima 10000EHF) with 16 h day photoperiod providing  $325 \mu\text{mol s}^{-1} \text{m}^{-2}$  of the photosynthetic photon flux density at plant level supplied by a mixture of incandescent bulbs and fluorescent lights. The temperature was set to 25 °C

during the light period and to 20 °C during the dark period, whereas relative humidity was maintained at 75% throughout the day and night. The standard solution for hydroponic growth included: 1.2 mM  $\text{KNO}_3$ ; 0.8 mM  $\text{Ca}(\text{NO}_3)_2$ ; 0.3 mM  $\text{MgSO}_4 \cdot 7\text{H}_2\text{O}$ ; 0.2 mM  $\text{NH}_4\text{H}_2\text{PO}_4$ ; 25 mM  $\text{CaCl}_2$ ; 25 mM  $\text{H}_3\text{BO}_3$ ; 0.5 mM  $\text{MnSO}_4$ ; 2 mM  $\text{ZnSO}_4 \cdot \text{H}_2\text{O}$ ; 0.5 mM  $\text{CuSO}_4 \cdot \text{H}_2\text{O}$ ; 0.5 mM  $\text{MoO}_3$ ; and 0.1 mM  $\text{NiSO}_4$ . Solutions were changed every five days.

During the first two weeks of hydroponic growth, all plants were supplemented with 20  $\mu\text{M}$  of Fe (III)-EDDHA [ethylenediamine-N,N’bis(o-hydroxyphenyl)acetic acid]. After the initial two weeks, plants were divided into two groups and different Fe conditions were imposed ( $n=15$  per Fe condition): Fe-sufficient plants [Fe+, supplemented with 20  $\mu\text{M}$  of Fe (III)-EDDHA] and Fe-deficient plants (Fe–, no Fe supplementation). Three Fe+ and three Fe– plants ( $n=3$ ) were collected for the analyses described below at the moment of Fe treatment application – 0 weeks after treatment (WAT) - and at 1, 2, 3 and 4 WAT.

### Mineral concentration analysis

Dried leaf samples of three plants per treatment, were collected at each timepoint, and dried at 60 °C until stable weight was obtained. Each sample was analysed for Fe, zinc (Zn), manganese (Mn), phosphorus (P), magnesium (Mg), calcium (Ca), and potassium (K) following the procedure described by Santos et al. (2020). Briefly, leaf samples were treated with an acid digestion procedure and mineral concentration determination was performed using the ICP-OES Optima 7000 DV (PerkinElmer, Waltham, MA, USA) with radial configuration.

Total N was quantified after sample combustion in an oxygen-rich high-temperature environment using the Dumatec 8000 Nitrogen Analyser (Foss Analytics, Denmark).

### Photosynthetic pigments quantification

Total chlorophyll, anthocyanin, and carotenoid concentrations were also evaluated. The different metabolites were extracted and quantified according to Sumanta et al. (2014), using a spectrophotometric method. The amount of each pigment ( $\mu\text{g g}^{-1}$  dry weight) was determined according to previously

published equations and having into account sample absorbances at 470, 652 and 665 nm (Nunes da Silva et al. 2020).

#### ABTS radical cation scavenging effect and DPPH scavenging assay

The extraction and analysis of the antioxidant activity by the 2-azino-bis-3-ethylbenzothiazoline-6-sulphonic acid (ABTS) radical scavenging assay was performed as described in Soares et al. (2021). In short, 500 mg of each sample was mixed with 10 ml of acetone/water/acetic acid (70:29.5:0.5, v/v/v), and incubated overnight in the dark with an orbital shaker. Samples were centrifuged at 1600 rpm for 10 min, and the supernatant was collected. After adjusting the daily ABTS working solution, with water, to an initial absorbance of 0.7 at 734 nm, 180  $\mu$ L of solution was added to 20  $\mu$ L of each sample, in a 96-well microplate. Mixtures reacted for 5 min in the dark and the absorbances were recorded at 734 nm in a microplate reader (Multiskan GO Microplate Spectrophotometer, Thermo Fisher Scientific Inc., Waltham, MA, USA).

The 2,2-diphenyl-1-picrylhydrazyl (DPPH) assay followed the procedure described in Vilas-Boas et al. (2020). Briefly, a working solution of 60  $\mu$ M DPPH was prepared in methanol and its absorbance was adjusted to 0.6 at 515 nm. An amount of 25  $\mu$ L of each sample was mixed with the DPPH working solution (175  $\mu$ L) and allowed to react in the dark for 30 min, at 25 °C in a 96-well microplate. Absorbances were measured at 515 nm. Trolox was used as the reference antioxidant to prepare a calibration curve for both assays. All assays were performed in duplicates.

#### Differential expression of Fe-related genes

Leaf tissue of three plants collected and frozen at each timepoint was individually pulverized thoroughly with a mortar and pestle until a fine powder was obtained, and total RNA was extracted using Qiagen RNeasy Mini Kit (#74,904) according to the manufacturer's instructions. RNA quality and quantity were checked using a nanophotometer. Single-stranded cDNA was then synthesized using iScript™ cDNA Synthesis Kit (Bio-Rad Laboratories Inc.), according to the manufacturer's instructions. Primer sequences were taken from Santos et al. (2016) (Table S1).

Quantitative PCR reactions were performed on a CFX96 Touch™ Deep Well Real-Time PCR Detection System (Bio-Rad Laboratories Inc.) using iQ™ SYBR Green Supermix (Bio-Rad Laboratories Inc.) with the following reaction conditions: 95 °C denaturation for 10 min; and 40 cycles with 15 s at 95 °C, 30 s at 54–56 °C (depending on primers used), followed by melt curve stages to check that only single products were amplified.

The comparative CT method ( $\Delta\Delta$ CT) was used for the relative quantification of gene expression using the geometric mean of the expression of the two stable reference genes as control transcripts and the plants grown with no added Fe as the reference sample. Two technical replicates were analysed and data were transferred to Excel files and plotted as histograms of normalized fold expression of target genes.

#### Infrared spectra acquisition

Infrared spectra of *G. max* leaves were obtained on a Fourier transform PerkinElmer Spectrum BX FTIR System spectrophotometer (USA) with a DTGS detector. Spectra were acquired in diffuse reflectance mode through a PIKE Technologies Gladi attenuated total reflectance (ATR) accessory within the wavenumber interval of 4000 to 600  $\text{cm}^{-1}$ , with a resolution of 4  $\text{cm}^{-1}$ . Each spectrum resulted from 32 scan co-additions. At each timepoint (0, 1, 2, 3 and 4 WAT), three plants (biological replicates) per treatment (Fe+ and Fe-) were used for infrared spectra acquisition in a total of  $5 \times 3 \times 2 = 30$  plants. Per plant, the middle foliate of the youngest trifoliate leaf, was selected and IR spectra of the adaxial side were acquired in two distinct spots in triplicate (instrumental replicates) in a total of  $30 \times 2 \times 3 = 180$  infrared spectra. In the first time point (0 WAT), spectra of the abaxial side of the plant leaves were also acquired for comparison purposes. Leaves were placed in the ATR crystal and a constant pressure was applied during spectral acquisition. The ATR crystal was cleaned and a background was acquired between each leaf.

#### Data analysis

To test for significant differences between Fe treatments, biological data were analysed as a completely randomized design using one-way ANOVA with

Fisher's LSD test, in GraphPad Prism 8 for macOS (GraphPad Software).

Spectral band intensities were obtained (after normalization) through integration *via* the "trapz" function of Matlab software. Peak ratios were obtained by dividing the corresponding integrated peak areas.

Spectra were modelled by principal component analysis (PCA) (Jolliffe 1986) and partial least square discriminant analysis (PLSDA) (Geladi and Kowalski 1986; Alsberg et al. 1998) to discriminate between Fe<sup>+</sup> and Fe<sup>-</sup> plants. Prior modelling, spectra of the two spots of the same leaf (three spectra x two spots) were averaged and pre-processed with standard normal variate (SNV) (Naes et al. 2002) and the Savitzky-Golay filter (n-smoothing points, 2nd polynomial order, and y-derivative order) and further mean centred. The PLSDA models were optimized: (I) for the spectral regions (15 distinct regions, defined in Fig. S1 of the supplementary material, alone and/or combined in the following manner: 1-Region R1; 2-Region R2; 3-Region R3; 4-Region R4; 5-Region R1 + R2 + R3 + R4; 6-Region R1 + R2; 7-Region R1 + R3; 8-Region R1 + R4; 9-Region R2 + R3; 10-Region R2 + R4; 11-Region R3 + R4; 12-Region R1 + R2 + R3; 13-Region R1 + R2 + R4; 14-Region R1 + R3 + R4; 15- Region R2 + R3 + R4); (II) spectra pre-processing method (Savitzky-Golay filter parameters: 9, 12, and 15 smoothing points and 1st and 2nd order derivative) (Steinier et al. 1972) and; (III) number of latent variables (LVs: 2, 3, 4 and 5).

For photosynthetic pigments (chlorophyll a, chlorophyll b, total chlorophyll, anthocyanins, and carotenoids), antioxidant activity (ABTS and DPHH scavenging effect), and mineral concentration estimates, partial least squares (PLS) regression models (Geladi and Kowalski 1986) were used. Prior to modelling, spectra were pre-processed with (SNV) (Naes et al. 2002) and Savitzky-Golay filter (9, 12, and 15 smoothing points, 2nd polynomial order, and 1st and 2nd order derivative) (Steinier et al. 1972) to remove baseline drifts and further mean centred. The number of LVs used were 3, 4, 5, 6, and 7. Before the development of the PLS models, spectra triplicates were averaged (three spectra obtained in the same leaf spot) and randomly divided into two independent data sets (70%/30%) to be used for the calibrations/cross-validation (70%) and for the validation (30%) of the PLS models. The division considered the

concentration range of the parameter to be estimated (spectra of both sets should cover the whole range). The accuracy of the models was evaluated by means of the coefficient of determination of calibration, cross-validation, and prediction ( $R^2C$ ,  $R^2CV$ , and  $R^2P$ ) and the root mean square error of calibration, cross-validation, and prediction (RMSEC, RMSECV, and RMSEP).

All chemometric models were performed in Matlab version 9.5 Release 2018b (MathWorks) and PLS Toolbox version 8.7 (2019) for Matlab (Eigenvector Research, Manson, WA).

## Results

### Mineral concentration analysis

Iron concentration (Fig. 1A) was significantly lower in Fe<sup>-</sup> plants as compared to Fe<sup>+</sup> plants at all time-points. Specifically, in Fe<sup>-</sup> plants it was lower by 45% (at 1 WAT), 64% (at 2 WAT), 79% (at 3 WAT), and 69% (at 4 WAT). Within the Fe<sup>-</sup> plants, Fe concentration decreased with time, being significantly lower at 2 WAT. In contrast, in Fe<sup>+</sup> plants, Fe concentration increased by more than double between 0 and 4 WAT ( $P < 0.0001$ ).

Zinc levels (Fig. 1B) were higher in Fe<sup>-</sup> plants than in Fe<sup>+</sup> plants (from 1 to 4 WAT). Between 0 and 2 WAT, Zn concentration significantly increased by 35% and then decreased at 3 WAT by 24%. In Fe<sup>+</sup> plants, Zn concentration significantly decreased from 0 to 4 WAT by 33%.

Manganese (Fig. 1C) was significantly higher in Fe<sup>-</sup> plants as compared to Fe<sup>+</sup> plants, at 1 and 2 WAT, by 53% and 138%, respectively. In Fe<sup>-</sup> plants, Mn concentration increased from 0 to 2 WAT by 94% ( $P < 0.001$ ) and decreased by 43% at from 2 to 3 WAT ( $P < 0.001$ ), while in Fe<sup>+</sup> plants, it had no significant changes.

The concentration of Ca (Fig. 2A) and Mg (Fig. 2B) showed similar trends. In general, Fe<sup>-</sup> plants had higher concentrations of both Ca and Mg, from 2 to 4 WAT. At 2 WAT, the concentration of these two elements significantly increased in Fe<sup>-</sup> plants, being higher than Fe<sup>+</sup> plants by 50% for Ca ( $P < 0.0001$ ) and by 28% for Mg ( $P < 0.01$ ).

The concentration of N (Fig. 2C) was always higher in Fe<sup>+</sup> plants from 1 WAT to 4 WAT. At 2

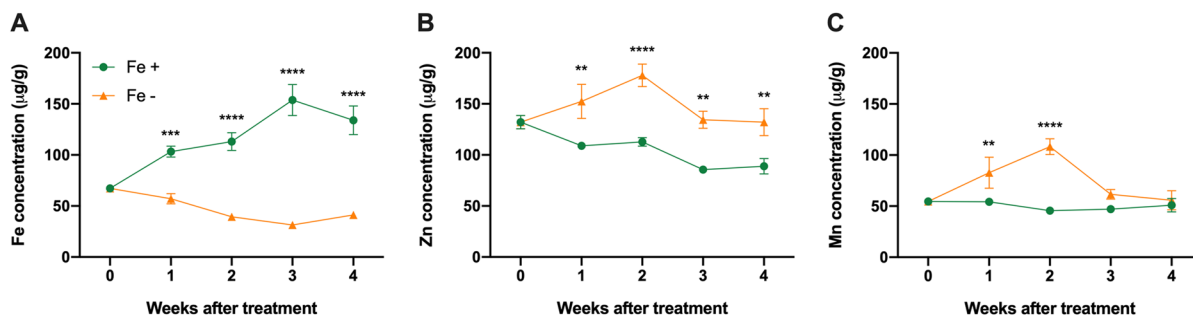


**Fig. 1** Iron (Fe, panel A), zinc (Zn, panel B) and manganese (Mn, panel C) leaf concentration of soybean plants. After two weeks of hydroponic growth with Fe supplementation, plants were divided into Fe sufficient (Fe+, green dots) and Fe deficient (Fe-, yellow triangles) conditions. Plants were sampled

at 0, 1, 2, 3, and 4 weeks after treatment imposition. Symbols represent the means of three biological replicates  $\pm$  SE. \*\*, \*\*\* and \*\*\*\* indicate significant differences between Fe treatments, at each time point, at  $P < 0.01$ ,  $P < 0.001$ , and  $P < 0.0001$ , respectively

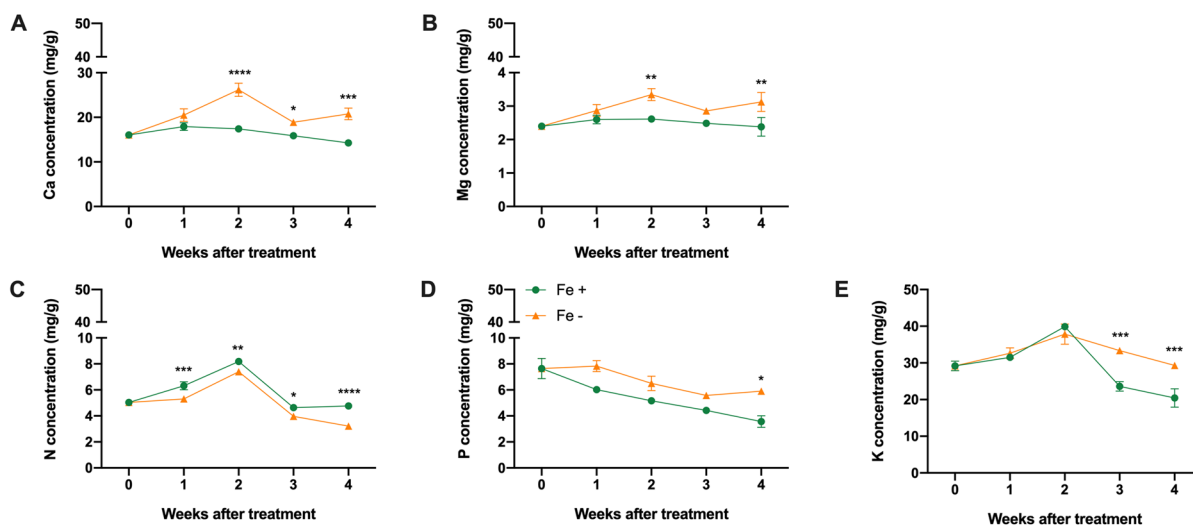


**Fig. 2** Calcium (Ca, panel A), magnesium (Mg, panel B), nitrogen (N, panel C), phosphorus (P, panel D), and potassium (K, panel E) leaf concentration of soybean plants. After two weeks of hydroponic growth with Fe supplementation, plants were divided into Fe sufficient (Fe+, green dots) and Fe deficient (Fe-, yellow triangles) conditions. Plants were sampled

at 0, 1, 2, 3, and 4 weeks after treatment imposition. Symbols represent the means of three biological replicates  $\pm$  SE. \*, \*\*, \*\*\* and \*\*\*\* indicate significant differences between Fe treatments, at each time point, at  $P < 0.05$ ,  $P < 0.01$ ,  $P < 0.001$ , and  $P < 0.0001$ , respectively

WAT, when compared to other timepoints, N concentration was highest both in Fe+ and Fe- plants ( $P < 0.0001$ ).

Regarding P (Fig. 2D), Fe- plants had higher P concentration than Fe+ plants by 66% ( $P < 0.05$ ), respectively. While P concentration was maintained throughout the assay in Fe- plants, in the

Fe+ plants it significantly decreased until the end of the assay ( $P < 0.001$ ).

For K concentration (Fig. 2E), both Fe- and Fe+ plants showed a significant increase from 0 to 2 WAT. After this timepoint, K concentration varied slightly in Fe- plants but significantly decreased in the Fe+ ones. Hence, Fe+ plants had lower K concentration by 41% at 3 WAT ( $P < 0.001$ ) and by 43% at 4 WAT ( $P < 0.001$ ), compared to Fe- plants.

## Photosynthetic pigments quantification

Total chlorophyll concentration (Fig. 3A) was significantly lower by 26% at 2 WAT and by 42% at 4 WAT in Fe<sup>-</sup> plants compared to Fe<sup>+</sup> plants. Within Fe<sup>-</sup> plants, total chlorophyll concentration didn't vary

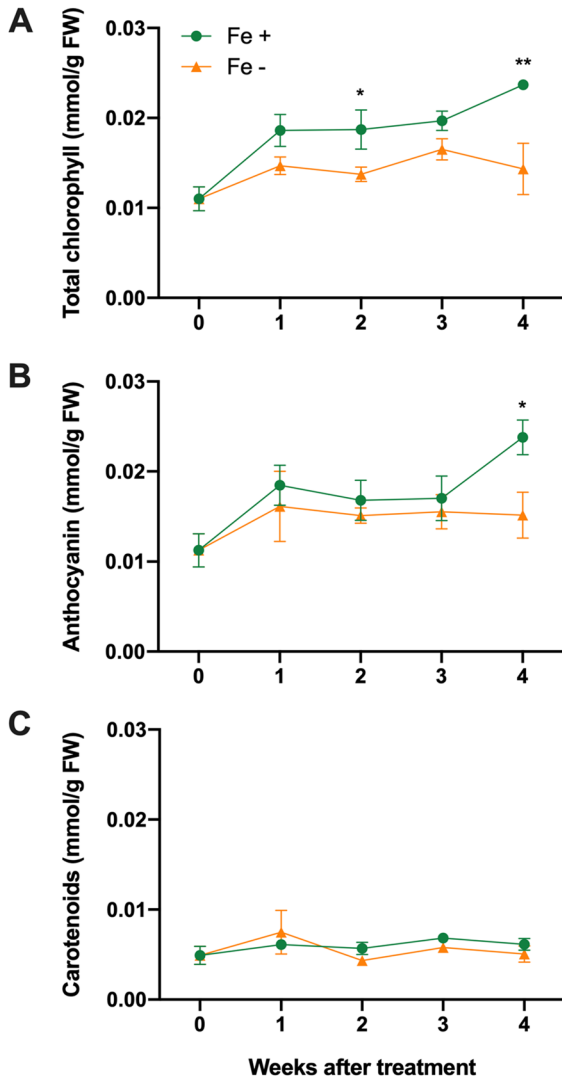


**Fig. 3** Total chlorophyll (A), anthocyanins (B), and carotenoids (C) concentrations in soybean leaves. After two weeks of hydroponic growth with Fe supplementation, plants were divided into Fe sufficient (Fe<sup>+</sup>, green dots) and Fe deficient (Fe<sup>-</sup>, yellow triangles) conditions. Plants were sampled at 0, 1, 2, 3, and 4 weeks after treatment imposition. Symbols represent the means of three biological replicates  $\pm$  SE. \* and \*\* indicate significant differences between Fe treatments, at each time point, at  $P < 0.05$ , and  $P < 0.01$ , respectively

between time points; however, in the Fe<sup>+</sup> plants, it significantly increased by 50% from 0 to 4 WAT ( $P < 0.001$ ).

Anthocyanins showed a similar trend to total chlorophyll concentration (Fig. 3B), where, in Fe<sup>-</sup> plants, anthocyanins concentration was significantly lower by 38% at 4 WAT compared to Fe<sup>+</sup> plants. The concentration of anthocyanins within Fe<sup>-</sup> plants didn't significantly change throughout the assay, but increased by 33% in Fe<sup>+</sup> plants from 0 to 4 WAT ( $P < 0.05$ ).

Carotenoid levels didn't significantly vary throughout the assay, both in Fe<sup>-</sup> and Fe<sup>+</sup> plants (Fig. 3C).

## Antioxidant activity

The antioxidant activity measured by the ABTS method (Fig. 4A) was 43% lower ( $P < 0.05$ ), at 2 WAT, in Fe<sup>-</sup> plants compared to Fe<sup>+</sup> plants.

The DPPH method (Fig. 4B) also showed that the antioxidant activity was lower in Fe<sup>-</sup> plants when compared to Fe<sup>+</sup> plants, from 2 to 4 WAT ( $P < 0.05$ ). Specifically, at 2 WAT, DPPH values significantly decreased in Fe<sup>-</sup> plants, being 36% lower than Fe<sup>+</sup> plants ( $P < 0.001$ ), while Fe<sup>+</sup> plants showed no significant changes throughout the assay.

## Gene expression

The relative expression of *FRO2*-like (Fig. 5A) and *IRT1*-like (Fig. 5B) genes was significantly higher in Fe<sup>-</sup> plants as compared to Fe<sup>+</sup> plants, at different time points. Specifically, in Fe<sup>-</sup> plants, *FRO2*-like gene expression was higher by 3.4-fold at 1 WAT ( $P < 0.01$ ), 3.7-fold at 2 WAT ( $P < 0.0001$ ), and 2.3-fold at 3 WAT ( $P < 0.01$ ); and *IRT1*-like gene by 2.7-fold at 1 WAT ( $P < 0.001$ ), 3.5-fold at 2 WAT ( $P < 0.0001$ ) and 2.0-fold at 3 WAT ( $P < 0.01$ ).

## Infrared spectra overview

Infrared spectra were obtained from the adaxial and abaxial parts of soybean leaves at 0 WAT. Two separate PCAs were conducted for each experimental condition (Fig. S2 in supplementary material). The resulting score maps showed no significant differences in the infrared profiles between the two sides, so only the adaxial part of the leaves was used for spectral acquisition in the subsequent weeks.

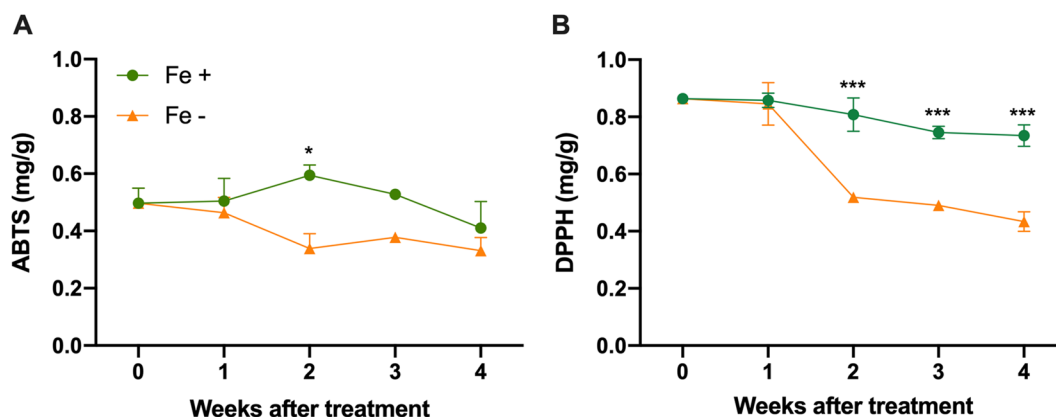


**Fig. 4** Antioxidant activity of soybean leaves by ABTS (2-azinobis-3-ethylbenzothiazoline-6-sulphonic acid) (A) and DPPH (2,2-diphenyl-1-picrylhydrazyl) (B) methods. After two weeks of hydroponic growth with Fe supplementation, plants were divided into Fe sufficient (Fe+, green dots) and Fe defi-

cient (Fe-, yellow triangles) conditions. Plants were sampled at 0, 1, 2, 3, and 4 weeks after treatment imposition. Symbols represent the means of three biological replicates  $\pm$  SE. \* and \*\*\* indicate significant differences between Fe treatments, at  $P < 0.05$ , and  $P < 0.001$ , respectively

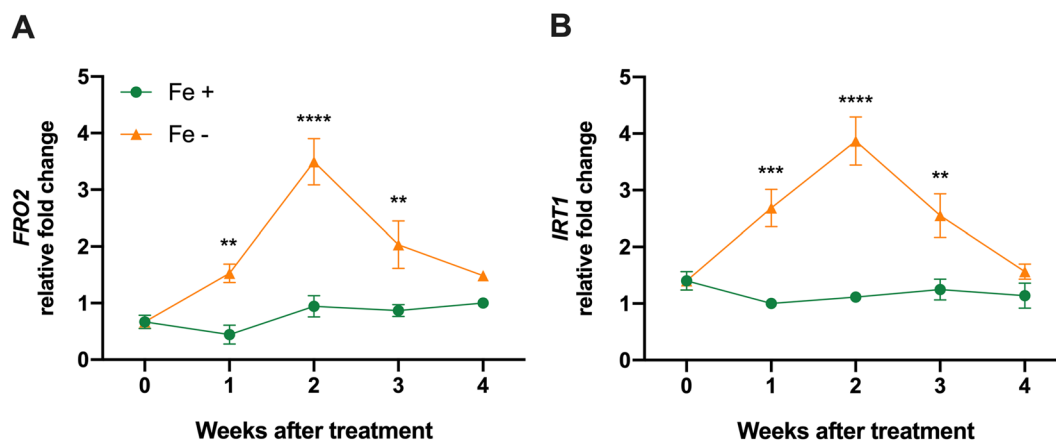


**Fig. 5** Relative gene expression of Ferric Reductase Oxidase 2 (FRO2, A) and Iron-Regulated Transporter 1 (IRT1, B) in soybean leaves. After two weeks of hydroponic growth with Fe supplementation, plants were divided into Fe sufficient (Fe+, green dots) and Fe deficient (Fe-, yellow triangles) conditions.

Plants were sampled at 0, 1, 2, 3, and 4 weeks after treatment imposition. Symbols represent the means of three biological replicates  $\pm$  SE. \*\*, \*\*\*, and \*\*\*\* indicate significant differences between Fe treatments, at each time point, at  $P < 0.01$ ,  $P < 0.001$ , and  $P < 0.0001$  respectively

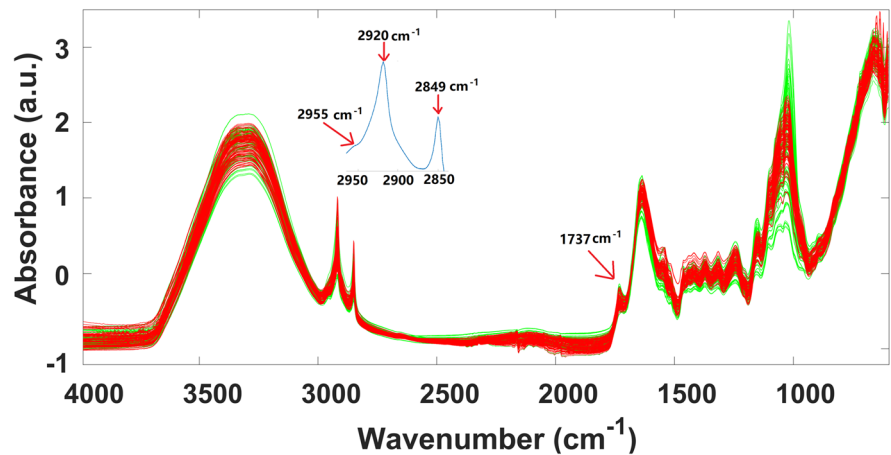
Figure 6 displays the FTIR-ATR spectra of Fe+ and Fe- plant leaves and their main components. Water content was identified by a broad peak at  $3400\text{ cm}^{-1}$  and peaks at  $1650\text{ cm}^{-1}$ . Absorption bands in the lipid region ( $2950\text{--}2850\text{ cm}^{-1}$ ) were identified, representing the plant waxes, cutin, and cutan; and a band in the carbonyl ester region ( $1750\text{--}1720\text{ cm}^{-1}$ ) ascribed to their esterified forms. The methylene:methyl ratio [ $(\text{---CH}_2\text{ asym} + \text{---CH}_2\text{ sym}) : \text{---CH}_3$ ] is frequently used to compare

the aliphatic chain length and branching degree of compounds with lipid nature among samples.

Figure S3 presents the integrated areas and ratios of absorption bands for all samples. The band vibrations areas in the lipid region ( $\text{---CH}_3$ ;  $\text{---CH}_2$  asymmetric;  $\text{---CH}_2$  symmetric and  $\text{C=O}$ ) slightly increased over time, indicating an increase in the content of wax, cutin, cutan, and their esterified forms (Fig. S3-A). However, there were no significant differences between Fe+ and Fe- plants over the weeks.



**Fig. 6** Infrared spectra of Fe sufficient (Fe+, green) and Fe deficient (Fe-, red) soybean leaves included in this study. Spectra were processed with SNV.



The methyl ratio [(—CH<sub>2</sub> asym + —CH<sub>2</sub> sym): —CH<sub>3</sub>] decreased throughout the study, especially in Fe+ plants, while Fe- plants' values stabilized around 3 WAT (Fig. S3-B). The degree of esterification increased in both Fe+ and Fe- plants from 0 to 1 WAT (Fig. S3-C).

The infrared spectra also showed typical absorption regions for protein and lipids (1700–1500 cm<sup>-1</sup>) and polysaccharides (1200–900 cm<sup>-1</sup>). To identify changes in these regions over time and between Fe+ and Fe- plants, the second derivative of the infrared signal was used (Fig. S4A-D in supplementary material). For Fe+ plants, the protein and polysaccharide absorption regions showed intensity alterations over the weeks (Figs S4-A and S4-B). The protein region had four main bands (1600, 1570, 1530, 1515 cm<sup>-1</sup>) with an increase from 0 to 2 WAT, then a small decrease or stabilisation from 2 to 4 WAT. The polysaccharide region had several absorption bands with an overall increase in intensity from 0 to 2 WAT (1020 cm<sup>-1</sup>), but less defined changes from 2 to 4 WAT. Fe- plants showed smaller variations in both absorption regions during the weeks (Fig. S4-C and S4-D). The vibration region between 1500–1200 cm<sup>-1</sup> was more difficult to infer variations as it includes vibrations from very different classes of compounds (lipids, proteins, among others).

Leaf biological parameters and mineral concentration estimates using IR profiles

Independent PLS regression models were developed to estimate the photosynthetic pigments (chlorophyll

a; chlorophyll b; total chlorophyll; anthocyanins and carotenoids), the antioxidant activity (ABTS and DPPH), and the mineral concentration for Fe+ and Fe- plants. 450 PLS models were obtained for each analyte per Fe treatment, corresponding to six combinations of the SavGol filter parameters (9,12,15 smoothing points x 1st and 2nd order derivative) X 5 tested LVs (3,4,5,6,7) x 15 spectral regions. Globally, 6300 PLS models were obtained and the optimum PLS models per condition are presented in Tables 1, 2 and 3.

Table 1 shows the figures of merit for PLS models developed to estimate photosynthetic parameters. The best models (lower RMSECV) were obtained using six LVs and the SavGol filter parameters (12,2,2) for the spectral region 1750–900 cm<sup>-1</sup>. Coefficients of determination for calibration were satisfactory (0.93–0.99), and cross-validation results were obtained for R<sup>2</sup>CV (>0.70) of chlorophyll a; total chlorophyll and anthocyanins for Fe+ samples, and of chlorophyll a and anthocyanins for Fe- samples. The correlation obtained in the cross-validation step for the remaining photosynthetic parameters was very poor (0.17–0.41). Prediction samples were satisfactory to estimate chlorophylls of Fe+ plants and chlorophyll a and anthocyanins of Fe- plants. The root means square errors were mainly below 5% for Fe+ plants, but errors were above 5% for cross-validation and prediction samples of Fe- samples.

Table 2 shows PLS models for antioxidant activity estimates. The best models were obtained using six LVs, the SavGol filter parameters (12,2,2) being the optimum spectral region for the estimates 1500–900 cm<sup>-1</sup>. The correlation coefficients for

**Table 1** Figures of merit obtained from the PLS regression models [6 LVs; SavGol (12,2,2); spectral region: 1750–900 cm<sup>-1</sup>] developed for Fe sufficient (Fe+) and Fe deficient (Fe-) plants, for photosynthetic parameters estimates

		RMSEC* (%)	R <sup>2</sup> C*	RMSECV* (%)	R <sup>2</sup> CV*	RMSEP* (%)	R <sup>2</sup> P*
Fe+	Chlorophyll a	0.7	0.98	2.0	0.87	1.4	0.87
	Chlorophyll b	1.3	0.97	6.6	0.41	3.9	0.70
	Total chlorophyll	1.1	0.96	2.3	0.82	1.5	0.89
	Anthocyanins	1.4	0.99	5.5	0.92	13.4	0.42
	Carotenoids	0.8	0.97	4.5	0.17	6.7	0.28
Fe-	Chlorophyll a	3.1	0.96	8.3	0.71	5.3	0.79
	Chlorophyll b	7.2	0.94	26.6	0.40	31.7	0.19
	Total chlorophyll	4.2	0.94	18.6	0.26	12.5	0.41
	Anthocyanins	2.1	0.98	6.1	0.86	10.9	0.88
	Carotenoids	6.5	0.93	24.3	0.25	21.5	0.59

\*RMSEC, RMSECV, RMSEP - root mean square error of calibration, cross-validation and prediction, respectively and the corresponding prediction determination coefficients (R<sup>2</sup>C, R<sup>2</sup>CV, R<sup>2</sup>P).

**Table 2** Figures of merit obtained from the PLS regression models [6 LVs; SavGol (12,2,2); spectral region: 1750–900 cm<sup>-1</sup>] developed for Fe sufficient (Fe+) and Fe deficient (Fe-) plants, for antioxidant activity estimates

		RMSEC* (%)	R <sup>2</sup> C*	RMSECV* (%)	R <sup>2</sup> CV*	RMSEP* (%)	R <sup>2</sup> P*
Fe+	ABTS	2.0	0.96	4.5	0.84	3.2	0.89
	DPPH	1.4	0.96	2.9	0.83	2.8	0.96
Fe-	ABTS	1.7	0.98	4.5	0.85	5.8	0.88
	DPPH	3.0	0.98	7.9	0.85	6.8	0.92

\*RMSEC, RMSECV, RMSEP- root mean square error of calibration, cross-validation and prediction, respectively and the corresponding prediction determination coefficients (R<sup>2</sup>C, R<sup>2</sup>CV, R<sup>2</sup>P)

**Table 3** Figures of merit obtained from the PLS regression models (6 LVs) developed for Fe sufficient (Fe+) and Fe deficient (Fe-) plants, for Fe, Zn, Mn, P, Mg, Ca and K concentration estimates

	Element	SavGol(n,x,y)	Spectral region (cm <sup>-1</sup> )	RMSEC* (%)	R <sup>2</sup> C*	RMSECV* (%)	R <sup>2</sup> CV*	RMSEP* (%)	R <sup>2</sup> P*
Fe+	P	12,2,2	3000–2800+1750–900	2.92	0.99	6.43	0.96	11.06	0.91
	K	12,2,2	3000–2800+1750–900	1.09	0.99	10.41	0.85	11.63	0.91
	Mg	15,2,1	1750–1200	0.31	0.99	0.73	0.94	2.35	0.69
	Ca	12,2,2	1750–1500+1200–900	0.61	0.99	2.57	0.91	6.93	0.78
	Fe	12,2,1	1500–900	2.12	0.99	5.68	0.96	13.42	0.86
	Mn	9,2,2	1750–1200	0.79	0.99	5.38	0.46	4.46	0.61
	Zn	12,2,1	1500–1200	1.70	0.99	3.55	0.94	4.91	0.88
Fe-	P	12,2,2	3000–2800+1750–900	2.56	0.97	5.64	0.61	9.70	0.78
	K	15,2,1	3000–2800+1750–900	0.95	0.97	9.08	0.80	10.14	0.76
	Mg	15,2,1	1750–1200	0.27	0.99	0.64	0.83	2.06	0.91
	Ca	12,2,2	1750–1500+1200–900	0.48	0.99	2.02	0.76	5.44	0.76
	Fe	12,2,1	1500–900	4.91	0.99	13.14	0.89	31.02	0.88
	Mn	9,2,2	1750–1200	0.55	0.99	3.71	0.91	3.08	0.86
	Zn	12,2,1	1500–1200	1.20	0.98	2.51	0.86	3.47	0.90

\*RMSEC, RMSECV, RMSEP- root mean square error of calibration, cross-validation and prediction, respectively and the corresponding prediction determination coefficients (R<sup>2</sup>C, R<sup>2</sup>CV, R<sup>2</sup>P)

ABTS and DPPH were very good (0.83–0.98), with errors below 5% for both Fe+ and Fe– plants, except for the cross-validation of DPPH (7.9%) and prediction of ABTS (5.8%) and DPPH (6.8%) of Fe– plants.

Table 3 displays PLS regression models for mineral concentration estimates, with the best model obtained for each nutrient by considering various spectral ranges and/or spectral pre-processing SavGol filter parameters. The determination coefficients for calibration sample sets were very satisfactory (all  $\geq 0.97$ ) for all nutrients and Fe treatments (Fe+ and Fe–), with RMSEC mostly below 1% and always below 5%.

The determination coefficients for calibration samples were satisfactory ( $\geq 0.97$ ), with RMSEC below 5%. For Fe+ plants,  $R^2CV$  was acceptable for all the nutrients (0.85–0.96) except for Mn (0.46), with RMSECV ranging from 0.73 to 10%. For Fe– plants,  $R^2CV$  was generally poorer (0.61–0.91) than the corresponding ones obtained for Fe+ plants. The RMSECV ranged from 0.64 to 13.14%. For Fe+ plants,  $R^2P$  was moderately satisfactory (0.78–0.91), with RMSEP ranging from 2 to 13%, except for Mn and Mg. For Fe– plants,  $R^2P$  was slightly better than for Fe+ ones (0.76–0.91), but the corresponding errors were poorer, with Fe estimate being very high (31%).

Discrimination between Fe sufficient and Fe deficient plants with FTIR

Multivariate data analysis was needed to differentiate between samples due to their global IR spectral

similarity. A PLSDA model was developed to discriminate between Fe+ and Fe– plants (Fig. 7), with a high percentage of correct class assignments (96.3%) achieved with five LVs in the spectral region 1200–900  $\text{cm}^{-1}$  and with a SavGol filter (12,2,1). The carbohydrate functional group vibrations dominated this spectral region. Table S3 depicts the percentages of correct class assignments obtained during the optimization step (corresponding to 360 PLSDA independent models developed). Spectra obtained at 0 WAT were not separated according to the Fe supplementation regimen, as this timepoint corresponds to the exact moment of the Fe treatment application and plants did not respond to it yet. From 1 WAT to the end of the study a clear separation between Fe-sufficient (green dots) and Fe-deficient (red triangles) was observed in the scores map supporting FTIR spectroscopy as an early IDC detection technique.

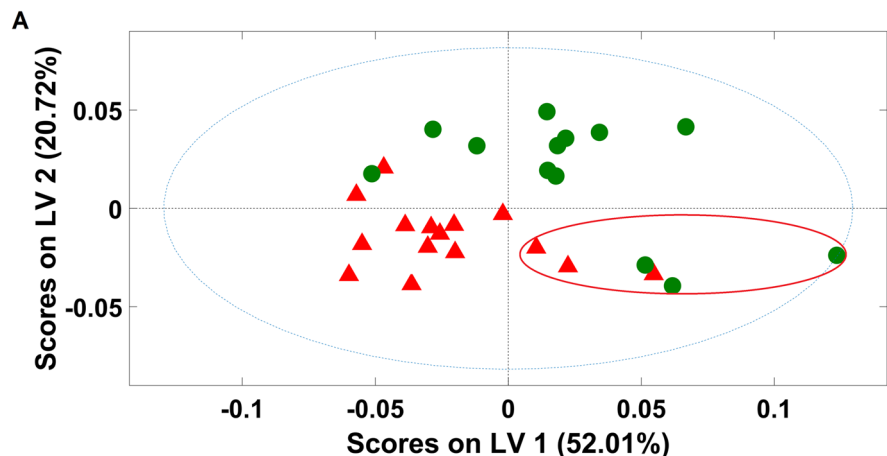
## Discussion

### Plant response to Fe deficiency stress

Soybean plants were grown under Fe-sufficiency for two weeks (0 WAT) before being divided into Fe-sufficient (Fe+) and Fe-deficient (Fe–) conditions and monitored for the four subsequent weeks (IR spectra acquisition and concomitant destructive biochemical and molecular analysis).

To confirm the different nutritional statuses of both groups of plants, Fe concentration was evaluated (Fig. 1A). While Fe+ plants had higher leaf Fe

**Fig. 7** Scores plot of the PLSDA regression model obtained for discrimination between Fe sufficient (Fe+, green dots) and Fe deficient (Fe–, red triangles) plants (A). The circle shows plants sampled at 0 weeks after treatment imposition



concentration and no chlorosis (Fig. 3A), Fe<sup>-</sup> plants maintained the initial Fe concentration (at 0 WAT) and unaltered pigment concentrations until 4 WAT. This suggests that the two initial weeks of hydroponic growth with Fe supplementation (prior to Fe stress treatment application) may have generated a Fe pool adsorbed to the roots or stored in the plant apoplast (Ye et al. 2022) that allowed them to maintain basal Fe levels for the whole assay. This Fe pool probably kept Fe<sup>-</sup> plants' photosynthetic machinery active (Shi et al. 2018), leading to unaltered levels of total chlorophyll, anthocyanin, and carotenoid concentration in Fe<sup>-</sup> leaves (Fig. 3). As Fe deficiency causes changes in cellular redox state and leads to ROS accumulation (Sun et al. 2016), the maintenance of photosynthetic pigments' concentration may be a strategy to reduce photo-oxidative damage in cells (Landi et al. 2015; Pérez-Gálvez et al. 2020; Santos et al. 2019b).

At 2 WAT (14 days of Fe-deficiency imposition), Fe concentration significantly decreased in Fe<sup>-</sup> plant leaves and their antioxidant activity was reduced (Fig. 4). Indeed, Atencio et al. (2021) showed that soybean leaves are more responsive to Fe stress after 10 days of Fe-deficiency imposition. As mentioned, Fe is a constituent of ROS-scavenging enzymes, and in its absence, plants' antioxidant capacity is impaired (Busch and Montgomery 2015; Prity et al. 2021). This fact is coherent with the decreased antioxidant activity registered herein.

At the transcriptional level, Fe deficiency induces the expression of FRO2 and IRT1 genes to mediate Fe uptake in plants (Riaz and Guerinot 2021). Herein, the expression levels of these two genes remained unchanged throughout the assay in Fe<sup>+</sup> plants, while in Fe<sup>-</sup> plants, they were significantly induced at 2 WAT, but decreased at 3 and 4 WAT (Fig. 5). This decrease may be a result of the tightly controlled signalling pathway to protect cells from metal toxicity under Fe deficiency (Kobayashi 2019). Under Fe-deficient conditions, IRT1 functions as a transporter of other divalent cations, such as Zn and Mn (Kaznina et al. 2019; Quintana et al. 2022). This explains the accumulation of these two minerals at 2 WAT in Fe<sup>-</sup> plants (Fig. 1B and C). However, the accumulation of non-Fe metal substrates leads to the degradation of IRT1, and although FRO2 is independent of this response, its activity is also affected by the dissociation of the complex responsible for Fe acquisition (Martín-Barranco et al. 2020). This might

explain the decrease both in FRO2 and IRT1 genes expression at 3 and 4 WAT, and in the leaf Zn and Mn concentration.

The modulation of plant status towards Fe regulation also impacted other non-metal elements, as previously described (Santos et al. 2015, 2019a). In the present study, the concentration of the macronutrients Ca, Mg, P and K was generally higher in Fe<sup>-</sup> plants, and responded to the Fe stress peak detected at 2 WAT (with the exception of P). Since Ca is also a divalent cation, Fe deficiency may result in a decrease in competition for Ca uptake and an increase in leaf Ca content (Bai et al. 2022; Fan et al. 2021). Also, Mg is a cofactor of photosynthetic enzymes and is involved in the tetrapyrrole cycle (Santos et al. 2019b). A specific cross-talk between Fe, P, and K signalling pathways has been reported (Wang et al. 2002), where Fe deficiency can affect these macronutrients uptake, assimilation and distribution, particularly at the mesophyll cells level (López-Millán et al. 2000).

The photosynthetic ability of plants is strongly correlated with the concentration of N, which is a vital component of chlorophylls, thylakoid proteins, and associated cofactors and enzymes (Perchlik and Tegeger 2018). It is also directly correlated to the leaf protein content (Mariotti et al. 2008). As expected, Fe<sup>+</sup> plants had higher amounts of leaf N, given that Fe deficiency leads to a decreased amount of nitrogen and amino acids, essential in protein synthesis (Borlotti et al. 2012; Cheng et al. 2019). Changes in leaf N were observed during the different plant development stages and at V3 (1 WAT) and V4 (2 WAT) there was an increase in leaf N content.

Overall, the analysed parameters indicate that the V3 and V4 vegetative stages are critical for soybean plants, as they coincide with increased growth and nutritional demand, as well as heightened sensitivity to Fe deficiency stress. Other studies have also shown that these are the growth stages when IDC symptoms are most pronounced in soybeans (Bai et al. 2018; Santos et al. 2021).

#### FTIR profiles and Fe deficiency prediction

Infrared absorption band profiles, intensities, and specific band ratios intensities can detect differences among crop leaf constituents and predict stress (Takehisa et al. 2022).

Herein, no differences were observed among IR spectra of the adaxial and abaxial sides of the leaf, likely due to leaf characteristics, contrary to previous reports in *Citrus* species and *Camellia japonica* (Páscoa et al. 2018, 2019; Sousa et al. 2019).

Absorption bands related to wax, cutin, and cutan had no intensity alterations between Fe+ and Fe- plants. Previous works reported a significant increase in waxes' content (and a further increase in the lipid region bands) in plants subjected to water stress (Kim et al. 2007). However, four IR bands in the protein absorption range (1600, 1570, 1530, 1515  $\text{cm}^{-1}$ ) presented remarkable intensity alterations throughout the assay: from 0 to 2 WAT, the Intensity of the bands increased, while from 2 to 4 WAT, they slightly decreased or stabilized. In the polysaccharides absorption region (1200–900  $\text{cm}^{-1}$ ) a similar trend was observed from 0 to 2 WAT. These results are coherent with those obtained for the stress indicators. Also, the increased band intensity for protein and polysaccharides absorption regions is compatible with plant growth in which a secondary cell wall formation occurs. Expansion proteins mediate the introduction of several polysaccharides in the leaves (cellulose, pectin, and hemicellulose), and contribute to more intense infrared bands (Yang and Yen 2002). Plants under Fe deficiency were generally smaller than the Fe+ plants (data not shown), which might correlate with leaf development stagnation due to cell wall organization under Fe stress conditions, as previously shown (Rodríguez-Celma et al. 2016; Soares et al. 2022).

The PLS models developed for predicting photosynthetic pigments globally performed well in calibration steps for both Fe+ and Fe- plants, with errors below 5% and  $R^2C > 0.93$ . However, chlorophyll b and carotenoids had poorly predicted parameters, particularly in Fe- plants, due to their lower concentration in these samples and higher stress and heterogeneity (Merry et al. 2021). PLS models developed for antioxidant activity (ABTS and DPPH) performed better than those for predicting photosynthetic pigments, with Fe- plants having the worst models. DPPH prediction were comparable to literature values for other plant species (Páscoa et al. 2019), with all analysed samples having RMSEC, RMSECV, and RMSEP values below 8%.

PLS models for estimating macro and micro-nutrients in soybean leaves showed robustness

for Fe+ plants, but lower accuracy for Mn, being coherent with other studies (Smith et al. 2014). For Fe- plants, the PLS models for Ca and P showed some lack of robustness. The FTIR spectra revealed increased lipid esterification in both Fe treatments during the first two weeks of the assay (Fig. 6). Other studies have shown that Fe deficiency induces lipid peroxidation due to the generation of ROS (Santos et al. 2019a, b, Sperotto et al. 2008, Teixeira et al. 2020), suggesting the ability to detect oxidative stress signals using FTIR spectroscopy.

Spectral analysis can detect Fe stress (Başayığit et al. 2015; Chi et al. 2009) and FTIR spectroscopy can predict other mineral stresses (Liu et al. 2014; van Maarschalkerweerd et al. 2013; Riaz et al. 2021). Herein, a PLS-DA model was used to distinguish between Fe+ and Fe- plants based on infrared spectra (Fig. 7). This separation was obtained from an early phase of stress induction, at 1 WAT (two independent clusters in the scores map). This confirms the ability of this technique to sense Fe stress from an early stage, even when no chlorosis symptoms were apparent (Fig. 3).

## Conclusion

Iron deficiency had a significant effect on the mineral concentration and gene expression in soybean plants only one week after Fe stress imposition, while the total chlorophyll and antioxidant activity were significantly impacted after two weeks of stress.

Specifically, after one week of Fe deficiency, the Fe- plants had lower Fe concentration and higher levels of Zn and Mn compared to the Fe+ plants. In addition, the Fe- plants had higher concentrations of Ca, Mg, and P, and lower N concentration throughout the entire assay.

The relative expression of FRO2-like and IRT1-like genes was significantly higher in Fe- plants compared to Fe+ plants at different time points, being highest at 2 WAT. After two weeks of Fe deficiency, Fe- plants had significantly lower total chlorophyll concentration compared to the Fe+ plants and the ABTS and DPPH results were significantly lower in Fe- plants compared to Fe+ plants.

Overall, these results advance the Fe nutrition mechanistic understanding by integrating the changes in mineral concentration, photosynthetic pigments,

antioxidant activity, and gene expression, allowing to highlight V3 and V4 growth stages as key developmental stages for IDC treatment and prevention. The use of spectral signatures as important early-on indices for observing alterations at the biochemical level of plants under Fe stress was reported. It was possible to detect Fe deficiency in plants with FTIR technology, allowing the selection of more efficient varieties for breeding purposes as well as the sustainable management of synthetic chelates application in the field.

**Acknowledgements** The authors would like to thank Elda Marsela for her support during the trial.

**Author contributions** Conceptualization: CSS, CS, MWV; Data curation: CSS, CS; Formal analysis: CSS, CS; Funding acquisition: MWV; Investigation: CSS, CS, MB, SP; Methodology: CSS, CS, MB, SP; Resources: MWV; Supervision: CSS, CS, MWV; Writing—original draft: CSS, CS; Writing—review & editing: MWV.

**Funding** Open access funding provided by FCTIFCCN (b-on). This work was supported by National Funds from FCT— Fundação para a Ciência e a Tecnologia through project UIDB/50016/2020 and 2022.01903.CEECIND.

**Data availability** The datasets generated during and/or analysed during the current study are available from the corresponding author upon reasonable request.

#### Declarations

**Competing interests** The authors have no relevant financial or non-financial interests to disclose.

**Open Access** This article is licensed under a Creative Commons Attribution 4.0 International License, which permits use, sharing, adaptation, distribution and reproduction in any medium or format, as long as you give appropriate credit to the original author(s) and the source, provide a link to the Creative Commons licence, and indicate if changes were made. The images or other third party material in this article are included in the article's Creative Commons licence, unless indicated otherwise in a credit line to the material. If material is not included in the article's Creative Commons licence and your intended use is not permitted by statutory regulation or exceeds the permitted use, you will need to obtain permission directly from the copyright holder. To view a copy of this licence, visit <http://creativecommons.org/licenses/by/4.0/>.

## References

- Akmakjian GZ, Riaz N, Guerinot ML (2021) Photoprotection during iron deficiency is mediated by the bHLH transcription factors PYE and ILR3. *Proc Natl Acad Sci USA* 118:40e2024918118. <https://doi.org/10.1073/pnas.2024918118>
- Alsberg BK, Kell DB, Goodacre R (1998) Variable selection in discriminant partial least-squares analysis. *Anal Chem* 70:4126–4133. <https://doi.org/10.1021/ac980506o>
- Atencio L, Salazar J, Lauter ANM, Gonzales MD, O'Rourke JA, Graham MA (2021) Characterizing short and long term iron stress responses in iron deficiency tolerant and susceptible soybean (*Glycine max* L. Merr). *Plant Stress* 2:100012. <https://doi.org/10.1016/j.stress.2021.100012>
- Bai G, Jenkins S, Yuan W, Graef GL, Ge Y (2018) Field-based scoring of soybean iron deficiency chlorosis using RGB imaging and statistical learning. *Front Plant Sci* 9:1002. <https://doi.org/10.3389/fpls.2018.01002>
- Bai R, Bai C, Han X, Liu Y, Yong JWH (2022) The significance of calcium-sensing receptor in sustaining photosynthesis and ameliorating stress responses in plants. *Front Plant Sci* 13:1019505. <https://doi.org/10.3389/fpls.2022.1019505>
- Başayığıt L, Dedeoğlu M, Akgül H (2015) The prediction of iron contents in orchards using VNIR spectroscopy. *Turk J Agric For* 39:123–134. <https://doi.org/10.3906/tar-1406-33>
- Borlotti A, Vigani G, Zocchi G (2012) Iron deficiency affects nitrogen metabolism in cucumber (*Cucumis sativus* L.) plants. *BMC Plant Biol* 12:189. <https://doi.org/10.1186/1471-2229-12-189>
- Breure TS, Haeefele SM, Hannam JA, Corstanje R, Webster R, Moreno-Rojas S, Milne AE (2022) A loss function to evaluate agricultural decision-making under uncertainty: a case study of soil spectroscopy. *Precis Agric* 23:1333–1353. <https://doi.org/10.1007/s11119-022-09887-2>
- Busch AWU, Montgomery BL (2015) Interdependence of tetrapyrrole metabolism, the generation of oxidative stress and the mitigative oxidative stress response. *Redox Biol* 4:260–271. <https://doi.org/10.1016/j.redox.2015.01.010>
- Butler HJ, McAinsh MR, Adams S, Martin FL (2015) Application of vibrational spectroscopy techniques to non-destructively monitor plant health and development. *Anal Methods UK* 7:4059–4070. <https://doi.org/10.1039/C5AY00377F>
- Ceballos-Laita L, Gutierrez-Carbonell E, Lattanzio G, Vázquez S, Contreras-Moreira B, Abadía A, Abadía J, López-Millán A-F (2015) Protein profile of *Beta vulgaris* leaf apoplastic fluid and changes induced by Fe deficiency and Fe resupply. *Front Plant Sci* 6:145. <https://doi.org/10.3389/fpls.2015.00145>
- Celletti S, Pii Y, Valentinuzzi F, Tiziani R, Fontanella MC, Beone GM, Mimmo T, Cesco S, Astolfi S (2020) Physiological responses to Fe deficiency in split-root tomato plants: possible roles of auxin and ethylene? *Agronomy* 10:1000. <https://doi.org/10.3390/agronomy10071000>

- Chaney RL (2022) Breeding soybeans to prevent mineral deficiencies or toxicities. In: Shibbes R (ed) World Soybean Research Conference III: Proceedings. CRC Press, Boulder, pp 453–459. <https://doi.org/10.1201/9780429267932>
- Cheng L, Zhang S, Yang L, Wang Y, Yu B, Zhang F (2019) Comparative proteomics illustrates the complexity of Fe, Mn and Zn deficiency-responsive mechanisms of potato (*Solanum tuberosum* L.) plants in vitro. *Planta* 250:199–217. <https://doi.org/10.1007/s00425-019-03163-w>
- Chi G, Chen X, Shi Y, Liu X (2009) Spectral response of rice (*Oryza sativa* L.) leaves to Fe<sup>2+</sup> stress. *Sci China Ser C-Life Sci* 52:747–753. <https://doi.org/10.1007/s11427-009-0103-7>
- Fan X, Zhou X, Chen H, Tang M, Xie X (2021) Cross-talks between macro- and micronutrient uptake and signalling in plants. *Front Plant Sci* 12:663477. <https://doi.org/10.3389/fpls.2021.663477>
- Feliciano RJ, Guzmán-Luna P, Boué G, Mauricio-Iglesias M, Hospido A, Membré J (2022) Strategies to mitigate food safety risk while minimizing environmental impacts in the era of climate change. *Trends Food Sci Technol* 126:180–191. <https://doi.org/10.1016/j.tifs.2022.02.027>
- Food and Agriculture Organization of the United Nations (2022) FAOSTAT: Crops and livestock products. <https://www.fao.org/faostat/en/#data/QCL>. Accessed 23 Sept 2022
- García MJ, Angulo M, Romera FJ, Lucena C, Pérez-Vicente R (2022) A shoot derived long distance iron signal may act upstream of the IMA peptides in the regulation of Fe deficiency responses in *Arabidopsis thaliana* roots. *Front Plant Sci* 29:971773. <https://doi.org/10.3389/fpls.2022.971773>
- García-Caparrós P, Filippis LD, Gul A, Hasanuzzaman M, Ozturk M, Altay V, Lao MT (2021) Oxidative stress and antioxidant metabolism under adverse environmental conditions: a review. *Bot Rev* 87:421–466. <https://doi.org/10.1007/s12229-020-09231-1>
- García-Marco S, Martínez ND, Yunta F, Hernández-Apaolaza L, Lucena J (2006) Effectiveness of ethylenediamine-N(o-hydroxyphenylacetic)-N'(p-hydroxyphenylacetic) acid (op-EDDHA) to supply iron to plants. *Plant Soil* 279(1–2):31–40. <https://doi.org/10.1007/s11104-005-8218-5>
- García-Mina JM, Bacaicoa E, Fuentes M, Casanova E (2013) Fine regulation of leaf iron use efficiency and iron root uptake under limited iron bioavailability. *Plant Sci* 198:39–45. <https://doi.org/10.1016/j.plantsci.2012.10.001>
- García-Molina A, Marino G, Lehmann M, Leister D (2020) Systems biology of responses to simultaneous copper and iron deficiency in *Arabidopsis*. *Plant J* 103:2119–2138. <https://doi.org/10.1111/tpj.14887>
- Geladi P, Kowalski BR (1986) Partial least-squares regression: a tutorial. *Anal Chim Acta* 185:1–17. [https://doi.org/10.1016/0003-2670\(86\)80028-9](https://doi.org/10.1016/0003-2670(86)80028-9)
- Guerinot ML, Yi Y (1994) Iron: nutritious, noxious and not readily available. *Plant Physiol* 104:815–820. <https://doi.org/10.1104/pp.104.3.815>
- Hassen TB, Bilali HE (2022) Impacts of the Russia-Ukraine war on global food security: towards more sustainable and resilient food systems? *Foods* 11:2301. <https://doi.org/10.3390/foods11152301>
- Hlahla JM, Mafa MS, Merwe R, Alexander O, Duvenhage M, Kemp G, Moloi MJ (2022) The photosynthetic efficiency and carbohydrates responses of six edamame (*Glycine max*. L. Merrill) cultivars under drought stress. *Plants* 11:394. <https://doi.org/10.3390/plants11030394>
- Jelali N, Wissal M, Dell'orto M, Abdelly C, Gharssali M, Zocchi G (2010) Changes of metabolic responses to direct and induced Fe deficiency of two *Pisum sativum* cultivars. *Environ Exp Bot* 68:238–246. <https://doi.org/10.1016/j.envexpbot.2009.12.003>
- Jeong J, Connolly EL (2009) Iron uptake mechanisms in plants: functions of the FRO family of ferric reductases. *Plant Sci* 176:709–714. <https://doi.org/10.1016/j.plantsci.2009.02.011>
- Jolliffe IT (1986) Principal component analysis. Springer-Verlag, New York. <https://doi.org/10.1007/978-1-4757-1904-8>
- Kaznina NM, Titov AF, Repkina NS, Batova YV (2019) Effect of zinc excess and low temperature on the IRT1 gene expression in the roots and leaves of barley. *Dokl Biochem Biophys* 487:264–268. <https://doi.org/10.1134/S1607672919040057>
- Kim KS, Park SH, Kim DK, Jenks MA (2007) Influence of water deficit on leaf cuticular waxes of soybean (*Glycine max* [L.] Merr). *Int J Plant Sci* 168:307–316. <https://doi.org/10.1086/510496>
- Kobayashi T (2019) Understanding the complexity of iron sensing and signaling cascades in plants. *Plant Cell Physiol* 60:1440–1446. <https://doi.org/10.1093/pcp/pcz038>
- Lahlali R, Jiang Y, Kumar S, Karunakaran C, Liu X, Borondics F, Hallin E, Bueckert R (2014) ATR-FTIR spectroscopy reveals involvement of lipids and proteins of intact pea pollen grains to heat stress tolerance. *Front Plant Sci* 5:747. <https://doi.org/10.3389/fpls.2014.00747>
- Landi M, Tattini M, Gould KS (2015) Multiple functional roles of anthocyanins in plant-environment interactions. *Environ Exp Bot* 119:4–17. <https://doi.org/10.1016/j.envexpbot.2015.05.012>
- Leite RS, Nascimento MN, Hernández-Navarro S, Potosme NMR, Karthikeyan S (2022) Use of ATR-FTIR spectroscopy for analysis of water deficit tolerance in *Physalis peruviana* L. *Spectrochim Acta A Mol Biomol Spectrosc* 280:121551. <https://doi.org/10.1016/j.saa.2022.121551>
- Lima MRM, Diaz SO, Lamego I, Grusak MA, Vasconcelos MW, Gil AM (2014) Nuclear magnetic resonance metabolomics of iron deficiency in soybean leaves. *J Prot Res* 13:3075–3087. <https://doi.org/10.1021/pr500279f>
- Liu G, Dong X, Liu L, Wu L, Peng S, Jiang C (2014) Boron deficiency is correlated with changes in cell wall structure that lead to growth defects in the leaves of navel orange plants. *Sci Hortic* 176:54–62. <https://doi.org/10.1016/j.scienta.2014.06.036>
- Liu N, Karunakaran C, Lahlali R, Warkentin T, Bueckert RA (2019) Genotypic and heat stress effects on leaf cuticles of field pea using ATR-FTIR spectroscopy. *Planta* 249:601–613. <https://doi.org/10.1007/s00425-018-3025-4>
- López-Millán AF, Morales F, Abadía A, Abadía J (2000) Effects of iron deficiency on the composition of the leaf apoplasmic fluid and xylem sap in sugar beet. Implications

- for iron and carbon transport. *Plant Physiol* 124(2):873–884. <https://doi.org/10.1104/pp.124.2.873>
- Mariotti F, Tomé D, Mirand PP (2008) Converting Nitrogen into Protein - Beyond 6.25 and Jones' factors. *Crit Rev Food Sci Nutr* 48:177–184. <https://doi.org/10.1080/10408390701279749>
- Martín-Barranco A, Spielmann J, Dubeaux G, Vert G, Zelazny E (2020) Dynamic control of the high-affinity iron uptake complex in root epidermal cells. *Plant Physiol* 184:1236–1250. <https://doi.org/10.1104/pp.20.00234>
- McCann MC, Hammouri M, Wilson R, Belton P, Roberts K (1992) Fourier transform infrared microspectroscopy is a new way to look at plant cell walls. *Plant Physiol* 100:1940–1947. <https://doi.org/10.1104/pp.100.4.1940>
- Mehmood S, Ahmed W, Ikram M, Imtiaz M, Mahmood S, Tu S, Chen D (2020) Chitosan modified biochar increases soybean (*Glycine max* L.) resistance to salt-stress by augmenting root morphology, antioxidant defense mechanisms and the expression of stress responsive genes. *Plants* 9:1173. <https://doi.org/10.3390/plants9091173>
- Merry R, Dobbels AA, Sadok W, Naeve S, Stupar RM, Lorenz AJ (2021) Iron deficiency in soybean. *Crop Sci* 62:36–52. <https://doi.org/10.1002/csc2.20661>
- Messina M, Sievenpiper JL, Williamson P, Kiel J, Erdman JW (2022) Perspective: soy-based meat and dairy Alternatives, despite classification as Ultra-processed Foods, deliver high-quality Nutrition on Par with unprocessed or minimally processed animal-based Counterparts. *Adv Nutr* 13:726–738. <https://doi.org/10.1093/advances/nmac026>
- Mittler R, Vanderauwera S, Gollery M, Van Breusegem F (2004) Reactive oxygen gene network of plants. *Trends Plant Sci* 9:490–498. <https://doi.org/10.1016/j.tplants.2004.08.009>
- Naes T, Isaksson T, Fearn T, Davies T (2002) A user-friendly guide to multivariate calibration and classification. NIR Publications, Chichester, UK
- Ncube E, Mohale K, Nogemane N (2022) Metabolomics as a prospective tool for soybean (*Glycine max*) crop improvement. *Curr Issues Mol Biol* 44:4181–4196. <https://doi.org/10.3390/cimb44090287>
- Nikalje GC, Kumar J, Nikam TD, Suprasanna P (2019) FT-IR profiling reveals differential response of roots and leaves to salt stress in a halophyte *Sesuvium portulacastrum* (L.) L. *Biotechnol Rep* 23:e00352. <https://doi.org/10.1016/j.btre.2019.e00352>
- Nunes da Silva M, Vasconcelos MW, Gaspar M, Balestra GM, Mazzaglia A, Carvalho SMP (2020) Early pathogen recognition and antioxidant system activation contributes to *Actinidia arguta* tolerance against *Pseudomonas syringae* pathovars actinidiae and actinidifoliorum. *Front Plant Sci* 11:1022. <https://doi.org/10.3389/fpls.2020.01022>
- Osman SOM, Saad AS, Tadano S, Takeda Y, Konaka T, Yamasaki Y, Tahir ISA, Tsujimoto H, Akashi K (2022) Chemical fingerprinting of heat stress responses in the leaves of common wheat by Fourier transform infrared spectroscopy. *Int J Mol Sci* 23:2842. <https://doi.org/10.3390/ijms23052842>
- Páscoa RNMJ, Moreira S, Lopes JA, Sousa C (2018) *Citrus* species and hybrids depicted by near and mid-infrared spectroscopy. *J Sci Food Agric* 98:3953–3961. <https://doi.org/10.1002/jsfa.8918>
- Páscoa RNMJ, Teixeira AM, Sousa C (2019) Antioxidant capacity of *Camellia japonica* cultivars assessed by near- and mid-infrared spectroscopy. *Planta* 249:1053–1062. <https://doi.org/10.1007/s00425-018-3062-z>
- Peiffer GA, King KE, Severin AJ, May GD, Cianzio SR, Lin SF, Lauter NC, Shoemaker RC (2012) Identification of candidate genes underlying an iron efficiency quantitative trait locus in soybean. *Plant Physiol* 158:1745–1754. <https://doi.org/10.1104/pp.111.189860>
- Perchlik M, Tegeder M (2018) Leaf amino acid supply affects photosynthetic and plant nitrogen use efficiency under nitrogen stress. *Plant Physiol* 178(1):174–188. <https://doi.org/10.1104/pp.18.00597>
- Pérez-Gálvez A, Viera I, Roca M (2020) Carotenoids and chlorophylls as antioxidants. *Antiox* 9:505. <https://doi.org/10.3390/antiox9060505>
- Prasad PVV (2003) Plant nutrition: iron chlorosis. In: Thomas B, Murphy DJ, Murray BG (eds) *Encyclopedia of applied plant sciences*. Elsevier Academic Press, London
- Prity SA, El-Shehawi AM, Elseehy MM, Tahura S, Kabir AH (2021) Early-stage iron deficiency alters physiological processes and iron transporter expression, along with photosynthetic and oxidative damage to sorghum. *Saudi J Biol Sci* 28:4770–4777. <https://doi.org/10.1016/j.sjbs.2021.04.092>
- Quintana J, Bernal M, Scholle M, Holländer-Czytko H, Nguyen NT, Piotrowski M, Mendoza-Cózatl DG, Haydon MJ, Krämer U (2022) Root-to-shoot iron partitioning in *Arabidopsis* requires iron-regulated transporter1 (IRT1) protein but not its iron(II) transport function. *Plant J* 109:992–1013. <https://doi.org/10.1111/tbj.15611>
- Riaz N, Guerinot ML (2021) All together now: regulation of the iron deficiency response. *J Exp Bot* 72:2045–2055. <https://doi.org/10.1093/jxb/erab003>
- Riaz M, Kamran M, El-Esawi MA, Hussain S, Wang X (2021) Boron-toxicity induced changes in cell wall components, boron forms, and antioxidant defense system in rice seedlings. *Ecotoxicol Environ Saf* 216:112192. <https://doi.org/10.1016/j.ecoenv.2021.112192>
- Rodríguez-Celma J, Lattanzio G, Villarrojo D, Gutierrez-Carbonell E, Ceballos-Laita L, Rencoret J, Gutiérrez A, del Río JC, Grusak MA, Abadía A, Abadía J, López-Millán A (2016) Effects of Fe deficiency on the protein profiles and lignin composition of stem tissues from *Medicago truncatula* in absence or presence of calcium carbonate. *J Proteom* 140:1–12. <https://doi.org/10.1016/j.jprot.2016.03.017>
- Santos CS, Roriz M, Carvalho SMP, Vasconcelos (2015) Iron partitioning at an early growth stage impacts iron deficiency responses in soybean plants (*Glycine max* L.). *Front Plant Sci* 6:325. <https://doi.org/10.3389/fpls.2015.00325>
- Santos CS, Carvalho SMP, Leite A, Moniz T, Roriz M, Rangel AOSS, Rangel M, Vasconcelos MW (2016) Effect of tris(3-hydroxy-4-pyridinonate) iron (III) complexes on iron uptake and storage in soybean (*Glycine max* L.). *Plant Physiol Biochem* 106:91–100. <https://doi.org/10.1016/j.plaphy.2016.04.050>
- Santos CS, Deuchande T, Vasconcelos MW (2019a) Molecular aspects of iron nutrition in plants. In Cánovas F, Lüttge



- U, Leuschner C, Risueño MC (eds) Progress in Botany 81:125–156. [https://doi.org/10.1007/124\\_2019\\_34](https://doi.org/10.1007/124_2019_34)
- Santos CS, Ozgur R, Uzilday B, Turkan I, Roriz M, Rangel AOSS, Carvalho SMP, Vasconcelos MW (2019b) Understanding the role of the antioxidant system and the tetrapyrrole cycle in iron deficiency chlorosis. *Plants* 8:348. <https://doi.org/10.3390/plants8090348>
- Santos CS, Silva B, Valente LMP, Gruber S, Vasconcelos MW (2020) The effect of sprouting in lentil (*Lens culinaris*) nutritional and microbiological profile. *Foods* 9:400. <https://doi.org/10.3390/foods9040400>
- Santos CS, Rodrigues E, Ferreira S, Moniz T, Leite A, Carvalho SMP, Vasconcelos MW, Rangel M (2021) Foliar application of 3-hydroxy-4-pyridinone Fe–chelate [Fe(mpp)<sub>3</sub>] induces responses at the root level amending iron deficiency chlorosis in soybean. *Physiol Plant* 173:235–245. <https://doi.org/10.1111/pp.13367>
- Shi R, Melzer M, Zheng S, Benke A, Stich B, von Wirén N (2018) Iron retention in root hemicelluloses causes genotypic variability in the tolerance to iron deficiency-induced chlorosis in maize. *Front Plant Sci* 9:557. <https://doi.org/10.3389/fpls.2018.00557>
- Singh N, Bhatla SC (2022) Heme oxygenase-nitric oxide cross-talk-mediated iron homeostasis in plants under oxidative stress. *Free Radic Biol Med* 182:192–205. <https://doi.org/10.1016/j.freeradbiomed.2022.02.034>
- Smith JP, Schmidtke LM, Müller MC, Holzapfel BP (2014) Measurement of the concentration of nutrients in grapevine petioles by attenuated total reflectance Fourier transform infrared spectroscopy and chemometrics. *Aust J Grape Wine Res* 20:299–309. <https://doi.org/10.1111/ajgw.12072>
- Soares JC, Zimmermann L, Santos NZ, Muller O, Pintado M, Vasconcelos MW (2021) Genotypic variation in the response of soybean to elevated CO<sub>2</sub>. *Plant-Environment Interact* 2:263–276. <https://doi.org/10.1002/pei3.10065>
- Soares JC, Osório H, Pintado M, Vasconcelos MW (2022) Effect of the interaction between elevated carbon dioxide and iron limitation on proteomic profiling of soybean. *Int J Mol Sci* 23:13632. <https://doi.org/10.3390/ijms232113632>
- Sousa C, Quintelas C, Augusto C, Ferreira EC, Páscoa RNMJ (2019) Discrimination of *Camellia japonica* cultivars and chemometric models: an interlaboratory study. *Comput Electron Agr* 159:28–33. <https://doi.org/10.1016/j.compag.2019.02.025>
- Sperotto RA, Boff T, Duarte GL, Fett JP (2008) Increased senescence-associated gene expression and lipid peroxidation induced by iron deficiency in rice roots. *Plant Cell Rep* 27:183–195. <https://doi.org/10.1007/s00299-007-0432-6>
- Steinier J, Termonia Y, Deltour J (1972) Smoothing and differentiation of data by simplified least squares procedure. *Anal Chem* 36:1627–1639. <https://doi.org/10.1021/ac60319a045>
- Sumanta N, Haque CI, Nishika J, Suprakrash R (2014) Spectrophotometric analysis of chlorophylls and carotenoids from commonly grown fern species by using various extracting solvents. *Res J Chem Sci* 4:63–69
- Sun C, Wu T, Zhai L, Li D, Zhang X, Xu X, Ma H, Wang Y, Han Z (2016) Reactive oxygen species function to mediate the Fe deficiency response in an Fe-efficient apple genotype: an early response mechanism for enhancing reactive oxygen production. *Front Plant Sci* 7:1726. <https://doi.org/10.3389/fpls.2016.01726>
- Takehisa H, Ando F, Takara Y, Ikehata A, Sato Y (2022) Transcriptome and hyperspectral profiling allows assessment of phosphorus nutrient status in rice under field conditions. *Plant Cell Environ* 45:1507–1519. <https://doi.org/10.1111/pce.14280>
- Teixeira GCM, Prado RM, Oliveira KS, Damião V, Junior GSS (2020) Silicon increases leaf chlorophyll content and iron nutritional efficiency and reduces iron deficiency in sorghum plants. *J Soil Sci Plant Nutr* 20:1311–1320. <https://doi.org/10.1007/s42729-020-00214-0>
- van Maarschalkerweerd M, Bro R, Egebo M, Husted S (2013) Diagnosing latent copper deficiency in intact barley leaves (*Hordeum vulgare*, L.) using near infrared spectroscopy. *J Agric Food Chem* 61:10901–10910. <https://doi.org/10.1021/jf402166g>
- Vilas-Boas AA, Campos DA, Nunes C, Ribeiro S, Nunes J, Oliveira A, Pintado M (2020) Polyphenol extraction by different techniques for valorisation of non-compliant portuguese sweet cherries towards a novel antioxidant extract. *Sustainability* 12:5556. <https://doi.org/10.3390/su12145556>
- Wang Y, Garvin DF, Kochian LV (2002) Rapid induction of regulatory and transporter genes in response to phosphorus, potassium, and iron deficiencies in tomato roots. Evidence for cross talk and root/rhizosphere-mediated signals. *Plant Physiol* 130:1361–1370. <https://doi.org/10.1104/pp.008854>
- Xu Z, Kurek A, Cannon SB, Beavis WD (2021) Predictions from algorithmic modelling result in better decisions than from data modelling for soybean iron deficiency chlorosis. *PLoS ONE* 16:e0240948. <https://doi.org/10.1371/journal.pone.0240948>
- Yang J, Yen HE (2002) Early salt stress effects on the changes in chemical composition in leaves of ice plant and *Arabidopsis*. A Fourier Transform Infrared Spectroscopy Study. *Plant Physiol* 130:1032–1042. <https://doi.org/10.1104/pp.004325>
- Ye JY, Zhou M, Zhu QY, Zhu YX, Du WX, Liu XX, Jin CW (2022) Inhibition of shoot-expressed NRT1.1 improves reutilization of apoplastic iron under iron-deficient conditions. *Plant J* 112:549–564. <https://doi.org/10.1111/tbj.15967>
- Yu S, Sheng L, Mao H, Huang X, Luo L, Li Y (2020) Physiological response of *Coryza Canadensis* to cadmium stress monitored by Fourier transform infrared spectroscopy and cadmium accumulation. *Spectrochim Acta A Mol Biomol Spectrosc* 229:118007. <https://doi.org/10.1016/j.saa.2019.118007>
- Zhitkovich A (2021) Ascorbate: antioxidant and biochemical activities and their importance for *in vitro* models. *Arch Toxicol* 95:3623–3631. <https://doi.org/10.1007/s00204-021-03167-0>

**Publisher's note** Springer Nature remains neutral with regard to jurisdictional claims in published maps and institutional affiliations.